



HAL
open science

DFT and $k^* p$ modelling of the phase transitions of lead and tin halide perovskites for photovoltaic cells

Jacky Even, Laurent Pedesseau, Jean-Marc Jancu, Claudine Katan

► To cite this version:

Jacky Even, Laurent Pedesseau, Jean-Marc Jancu, Claudine Katan. DFT and $k^* p$ modelling of the phase transitions of lead and tin halide perovskites for photovoltaic cells. *physica status solidi (RRL)* - Rapid Research Letters, 2014, 8 (1), pp.31-35. 10.1002/pssr.201308183 . hal-00920121

HAL Id: hal-00920121

<https://hal.science/hal-00920121v1>

Submitted on 17 Dec 2013

HAL is a multi-disciplinary open access archive for the deposit and dissemination of scientific research documents, whether they are published or not. The documents may come from teaching and research institutions in France or abroad, or from public or private research centers.

L'archive ouverte pluridisciplinaire **HAL**, est destinée au dépôt et à la diffusion de documents scientifiques de niveau recherche, publiés ou non, émanant des établissements d'enseignement et de recherche français ou étrangers, des laboratoires publics ou privés.

DFT and $k \cdot p$ modelling of the phase transitions of lead and tin halide perovskites for photovoltaic cells

Jacky Even^{*1}, Laurent Pedesseau¹, Jean-marc Jancu¹, and Claudine Katan,²

¹ Université Européenne de Bretagne, INSA-FOTON-UMR 6082, 35708 Rennes, France

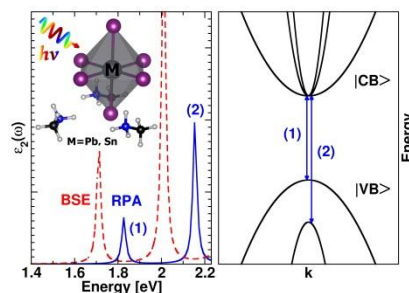
² CNRS, Institut des Sciences Chimiques de Rennes, UMR 6226, 35042 Rennes, France

Keywords Perovskite, photovoltaic, first-principles calculations, $k \cdot p$, spin-orbit coupling

* Corresponding author: e-mail Jacky.Even@insa-rennes.fr, Phone: +33 (0)2 23 23 82 95, Fax: +33 (0)2 23 23 86 18

3D hybrid organic perovskites, $\text{CH}_3\text{NH}_3\text{PbX}_3$ (X=halogen), have recently been used to strongly improve the efficiency of dye sensitized solar cells (DSSC) leading to a new class of low-cost mesoscopic solar cells. CsSnI_3 perovskite can also be used for hole conduction in DSSC. Density functional theory is used to compare lead and tin hybrid and all-inorganic perovskites. The band ordering is reversed as compared to conventional semiconductors. The room temperature optical absorption is associated to electronic transitions between the spin-orbit split-off band in the conduction band and the valence band. Spin-orbit coupling is about three times smaller for tin. Moreover, the effective mass of relevant band edge hole states is small (0.17). The high temperature phase sequence of CsSnI_3 leading to the room temperature orthorhombic phase and the recently reported phases of $\text{CH}_3\text{NH}_3\text{MI}_3$ (where M=Pb, Sn) close to the room temperature, are also studied. Tetragonal distortions from the ideal cubic phase, are analysed by a $k \cdot p$ perturbation, in-

cluding spin-orbit effect. In addition, the non centrosymmetric phases of $\text{CH}_3\text{NH}_3\text{MI}_3$ exhibit a splitting of the electronic bands away from the critical point. The present work shows that their physical properties are more similar to conventional semiconductors than to the absorbers used in DSSC.



1 Introduction Over the past decade, Hybrid Organic/inorganic Perovskites (HOPs) have attracted increasing interest in the field of optoelectronics [1] and more recently for solar cells [2,3], thanks to their ease of synthesis, opening new routes for low-cost technologies. Reduced costs and higher conversion efficiencies are indeed of crucial importance to make photovoltaic technologies a reliable choice to cover emerging energy needs [4]. The quest for higher conversion efficiencies mainly relies on semiconductor heterostructures such as high-performance III-V/silicon multiple junctions cells [5], that require high level technologies. Following pioneering works [2, 3], three-dimensional (3D) HOPs like $\text{CH}_3\text{NH}_3\text{PbX}_3$ (where X=I, Br, Cl), have recently emerged as a novel class of low-cost materials for solid-state mesoscopic solar cells [6-10], where an efficiency of 20% is predicted [11]. Structure and internal

mechanisms of these hybrid semiconductor photovoltaic cells (HSPC) may differ from the one of dye-sensitized solar cells (DSSC) [12]. Interestingly, the organic part provides a structural flexibility that makes these materials appealing for mesostructured HSPC, but it also yields structural disorder. The design of novel devices with enhanced responses can benefit from predictive modelling of these HOPs using Density Functional Theory (DFT). Surprisingly, despite the important relativistic effects expected for lead tin in HOP, spin-orbit coupling (SOC) effects have been overlooked until recently from the theoretical point of view [13, 14]. Moreover, concepts from solid-state physics may be used for HOPs to reach the level of knowledge already attained for the optoelectronic properties of conventional semiconductors. In fact, it has been demonstrated that the band ordering of 3D [13] and 2D [14] HOPs close

to the band gap is reversed when compared to conventional semiconductors. In addition, the critical electronic transition is dominated by a giant SOC in the conduction band (CB) [13, 14]. GW many-body corrections to DFT have clearly demonstrated that the agreement previously reported between calculated and experimental band gaps is fortuitous, and stems from error cancellation between SOC and many-body effects [13].

All-inorganic analogues of such HOPs, namely CsSnI_3 , have also been reported for hole conduction in lieu of a liquid electrolyte in DSSC [15]. It is also presumed to take part in light absorption on the red side of the solar spectrum [16]. These compounds have a high temperature cubic phase (Pm3m) that can be considered as an ideal reference structure to understand the basic electronic properties of related HOPs and all-inorganic analogues [13, 17]. However, one should also consider more realistic situations such as the room temperature orthorhombic γ -phase of CsSnI_3 , which differs significantly from the ideal cubic α -phase of CsSnX_3 and CsPbX_3 [18, 19].

Until recently, it was considered that 3D HOPs crystallise in a high-temperature cubic phase with dynamical disorder of the organic cations CH_3NH_3^+ [20, 21, 22]. Very recently, Single crystal X-ray diffraction analysis led to a refinement of the structures of $\text{CH}_3\text{NH}_3\text{MI}_3$ (where $\text{M}=\text{Pb}, \text{Sn}$) close to the room temperature [23]. Their high temperature phases correspond to a non-centrosymmetric tetragonal P4mm structure, slightly strained from the ideal cubic Pm3m phase, where carbon and nitrogen atoms can be located. Both compounds exhibit a phase transition to a tetragonal non-centrosymmetric and centered I4cm phase. For the technologically important HOP, $\text{CH}_3\text{NH}_3\text{PbI}_3$, this transition occurs above room temperature ($T_c=333\text{K}$). In the previously reported room temperature centrosymmetric tetragonal I4mcm phase of $\text{CH}_3\text{NH}_3\text{PbI}_3$, carbon and nitrogen atoms were indeed not properly located on Wyckoff positions [22]. In addition, crystallographic data of the orthorhombic low temperature phases of $\text{CH}_3\text{NH}_3\text{MX}_3$ are also available [21, 24].

In this work, thanks to DFT and \mathbf{k}, \mathbf{p} approaches, we investigate the properties of different phases of tin and lead based HOPs and their all-inorganic analogues. First, we start by considering the high temperature cubic α -phase of all-inorganic compounds, and the phase sequence of CsSnI_3 that leads to a room temperature orthorhombic phase. Then, we investigate different phases of both $\text{CH}_3\text{NH}_3\text{PbI}_3$ and $\text{CH}_3\text{NH}_3\text{SnI}_3$ using the latest crystal data. We systematically consider SOC and propose a perturbative analysis of the electronic band structure, including strain effects. This \mathbf{k}, \mathbf{p} model is applied to tetragonal phases. The effect of non-centrosymmetry on the band diagram is also explored.

2 Methods

Calculations were performed using the DFT implementation available in the ABINIT pseudo-potential package

[25] with the LDA for exchange-correlation and relativistic, norm-conserving, separable, dual-space Gaussian-type pseudopotentials for all atoms [26] in order to include the spin-orbit coupling. The electronic wave-functions are expanded onto a plane-wave basis set with an energy cut-off of 950 eV. The GW self-energy perturbation was performed within ABINIT after a LDA computation without SOC. The study of the cubic phases was also performed with the FP-LAPW Elk code [27] at the GGA-level [28]. The Bethe-Salpeter equation (BSE) was solved for the cubic phase [29]. The dielectric constant was also determined within the Random-Phase Approximation (RPA). $4 \times 4 \times 4$ Monkhorst-Pack grids are used for reciprocal space integration, except for the cubic phases ($8 \times 8 \times 8$). It has been previously shown that the band structure of HOPs close to the band gap may be reproduced by replacing the organic cation by Cs^+ located at the nitrogen position [13].

3 Results and discussion

3.1 Electronic properties of CsSnI_3 and CsPbI_3 cubic phases The electronic properties of the high temperature cubic α -phase of CsSnI_3 have already been studied without SOC by DFT plane wave pseudopotential approach [17]. These results showed that the optical ground state transition is related to a direct electronic transition located at the R-point of the Brillouin zone, leading to a band gap of 0.35 eV for CsSnI_3 [17]. It is worth mentioning that even though SOC was neglected, the agreement with the measured band gap at room temperature (1.3 eV, [15, 16, 23]) is poor. Similar calculations for the room temperature orthorhombic γ -phase of CsSnI_3 led to a somewhat higher value (0.56 eV) [17]. The inclusion of SOC, has been recently reported for CsPbX_3 ($\text{X}=\text{I}, \text{Br}$) [13], showing that SOC cannot be disregarded for lead halide perovskites.

Figure 1 shows a comparison of the electronic structure of CsSnI_3 and CsPbI_3 without and with SOC using an all-electron FP-LAPW approach. In both cases, the band gap is located at the R-point and the CB critical states correspond to a triply degenerate odd states without SOC and a twice-degenerate spin-orbit split-off states with SOC:

$$E_{1,2} = E_{CB}^0 + \Delta_{SO}/3$$

$$E_{3(SO)} = E_{CB}^0 - 2\Delta_{SO}/3$$

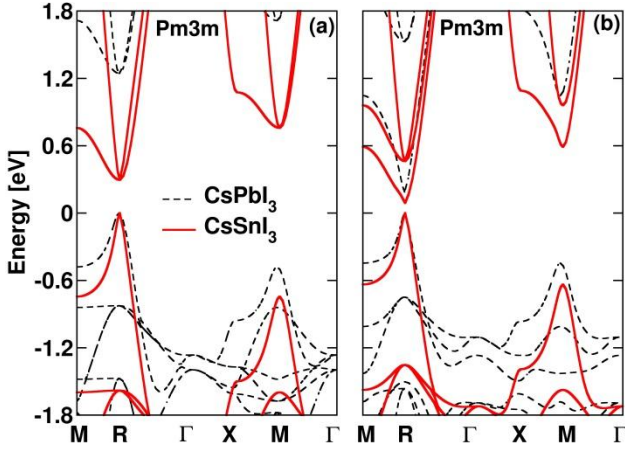


Figure 1 Comparison of the electronic band diagram of cubic CsSnI₃ (red straight lines) and CsPbI₃ (black dotted lines) without (a) and with (b) SOC.

The SOC splitting in CsSnI₃ is about $\Delta_{so} \approx 0.4\text{eV}$, three times smaller than the corresponding one in CsPbI₃ [13]. The hole effective masses can be evaluated from the valence band (VB) hole dispersion curve with a small warping ($m_{eff} \approx 0.12$ and 0.04 respectively for CsPbI₃ and CsSnI₃). The CsSnI₃ band gap with (without) SOC amounts to 0.1eV (0.3eV). Similar results are obtained within a plane wave pseudopotential method [25]. A one-shot many-body (GW) corrections to the LDA gap of CsSnI₃ (without SOC) amounts to 0.6eV . This correction is similar to that obtained for CsPbI₃ [13]. It is not sufficient to recover the measured optical band gap (1.3eV). Indeed more involved many-body techniques should be used and excitonic effects cannot be neglected. Besides it is well-known that band gaps and effective masses are related [29]. Based on experimental band gaps [23], hole effective masses of both tin and lead compounds become comparable (0.17).

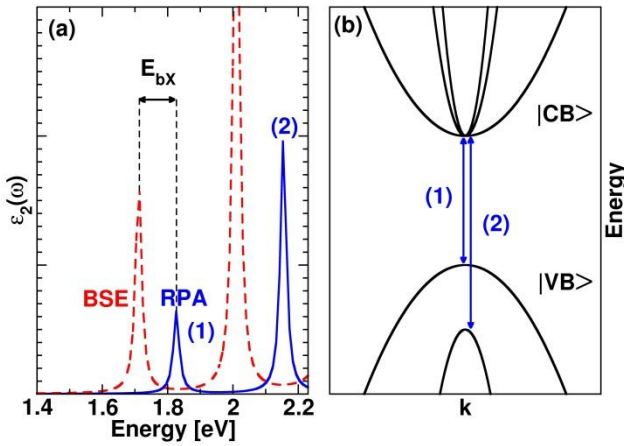


Figure 2 (a) Comparison of the dielectric constant variation of CsPbI₃ with (red dotted line, BSE calculation) and without (blue straight line, RPA calculation) the excitonic interaction. (b) Schematic representation of the two optical transitions.

Figure 2 shows the dielectric constant of CsPbI₃ calculated without SOC, including a scissor correction of 0.6eV for the band gap. The first absorption peak, located at about 1.8eV , corresponds to the fundamental transition between the triply degenerate CB state and the VB state (blue line, RPA level). From a BSE computation (red line), it is found that excitonic interaction enhances the absorption with a sizeable binding energy ($E_{bX} \approx 0.1\text{eV}$).

3.2 Phase transitions and room temperature orthorhombic phase of CsSnI₃ On cooling at 426K , the crystal converts to a $P4/m\text{b}m$ tetragonal β -phase [15], with a cell doubling perpendicular to the tetragonal axis. The corresponding strain tensor holds $\epsilon_{xx} = \epsilon_{yy} = -0.14\%$ and $\epsilon_{zz} = 0.28\%$.

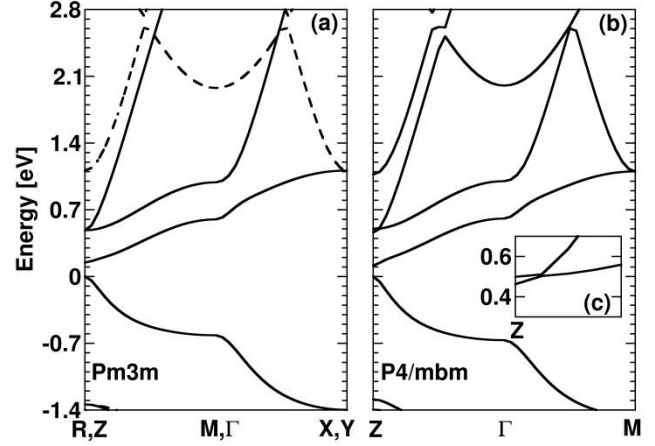


Figure 3 Band structure of CsSnI₃ with SOC (a) from folded bands of the cubic α -phase (straight line, along R-M and dotted line along Z- Γ) (b) for the tetragonal $P4/m\text{b}m$ β -phase. (c) Insert shows the small splitting due to tetragonal strain near the Z-point.

To highlight the changes of the band structure during this phase transition, figure 3 compares the bands of the tetragonal phase with folded bands derived from the cubic phase. The insert illustrates the small splitting induced by the tetragonal strain on the CB states. This effect can be first analysed without SOC within a $\mathbf{k}\cdot\mathbf{p}$ approach close to the R-point. The corresponding \mathbf{k} -dependent Hamiltonian for the triply degenerate CB reads:

$$H_{\mathbf{k}} = E_{CB}^0 + \begin{pmatrix} Lk_x^2 + M(k_y^2 + k_z^2) & Nk_x k_y & Nk_x k_z \\ Nk_x k_y & Lk_y^2 + M(k_x^2 + k_z^2) & Nk_y k_z \\ Nk_x k_z & Nk_y k_z & Lk_z^2 + M(k_x^2 + k_y^2) \end{pmatrix}$$

Influence of strain can be treated perturbatively:

$$H_{\epsilon} = \begin{pmatrix} l\epsilon_{xx} + m(\epsilon_{yy} + \epsilon_{zz}) & n\epsilon_{xy} & n\epsilon_{xz} \\ n\epsilon_{xy} & l\epsilon_{yy} + m(\epsilon_{xx} + \epsilon_{zz}) & n\epsilon_{yz} \\ n\epsilon_{xz} & n\epsilon_{yz} & l\epsilon_{zz} + m(\epsilon_{xx} + \epsilon_{yy}) \end{pmatrix}$$

The $E_{CB}^0, M, L, N, l, m, n$ can be extracted either from experiment [30] or from state of the art electronic structure calculations [31].

At the R(Z)-point of CsSnI_3 , the energy splitting $\delta E = (\mathbf{l} - \mathbf{m})(\epsilon_{xx} - \epsilon_{zz})$ can be evaluated from our DFT computation without SOC leading to $(\mathbf{l} - \mathbf{m}) \approx -1eV$.

The SOC can be further added perturbatively, considering spinor states (figures 1, 3). The three eigenvalues of the total Hamiltonian are doubly degenerated and given by:

$$E_0 = E_{CB}^0 + \delta E + \Delta_{SO}/3$$

$$E_{\pm} = E_{CB}^0 + \frac{\delta E - \Delta_{SO}/3}{2} \pm \sqrt{\left(\frac{\delta E - \Delta_{SO}/3}{2}\right)^2 + 2\Delta_{SO}^2/9}$$

In the particular case of the $\text{Pm}\bar{3}\text{m}$ - $\text{P4}/\text{mbm}$ transition of CsSnI_3 , SOC is larger than strain effect $\Delta_{SO}/3 \gg \delta E$ (figure 3) and:

$$E_+ \approx E_{CB}^0 + \Delta_{SO}/3, E_- \approx E_{CB}^0 + \delta E - 2\Delta_{SO}/3$$

This shows that detailed analysis of the effect of the phase transitions on the electronic properties must involve SOC. The room temperature orthorhombic $\text{Pnma}\gamma$ -phase is derived from the $\text{P4}/\text{mbm}\beta$ -phase by a cell doubling along the c-axis [15]. This leads to an additional folding from the Z-point of the β -phase to the Γ -point of the γ -phase. The SOC effect is again larger than the strain one. The splitting of the SO band with the next CB is equal to 0.4eV, consistently with earlier findings [15].

3.3 Interplay of SOC and loss of inversion symmetry in $\text{CH}_3\text{NH}_3\text{PbI}_3$ and $\text{CH}_3\text{NH}_3\text{SnI}_3$ Earlier DFT calculations including SOC were already performed for $\text{CH}_3\text{NH}_3\text{PbI}_3$, but using available structural data for the α, β, γ -phases [13]. Recent crystallographic data [23] allow to investigate further the high temperature α -phase of $\text{CH}_3\text{NH}_3\text{MI}_3$ HOPs. It is characterized by a tetragonal P4mm structure, slightly strained from the ideal cubic $\text{Pm}\bar{3}\text{m}$ phase ($\epsilon_{zz} = 0.04$ and 0.01% for $\text{M} = \text{Pb}$ and Sn , respectively). The band diagram is similar to that reported for the cubic phase of CsPbI_3 (figure 1). The SOC splitting is equal to 1.5 and 0.4eV for $\text{M} = \text{Pb}$ and Sn , respectively. Hole effective masses evaluated from the VB dispersion are found similar to that obtained for CsPbI_3 and CsSnI_3 . The most important feature is due to the loss of the inversion symmetry that induces a splitting of the bands away from the critical point. The electronic band diagram of the P4mm phase of both $\text{CH}_3\text{NH}_3\text{MI}_3$ HOPs close to the A-point (corresponding to the R-point of the ideal cubic phase) indeed exhibits a small splitting of the bands.

This effect is more important for the tetragonal I4cm β -phase in both compounds (figure 4). The bands are folded from the A-point to the Γ -point (figure 4). The α - β phase transition is associated to a group-subgroup relationship between P4mm and I4cm . It is similar to the previously proposed $\text{Pm}\bar{3}\text{m}$ - $\text{I4}/\text{mcm}$ phase sequence [20-22] analysed without inversion asymmetry for $\text{CH}_3\text{NH}_3\text{PbI}_3$ [13]. We underline that the previous DFT calculations for the γ -phase of $\text{CH}_3\text{NH}_3\text{PbI}_3$ [13] were performed using a refined centrosymmetric orthorhombic Pnma structure [21]. However the structure of the γ -phase of $\text{CH}_3\text{NH}_3\text{MI}_3$ com-

pounds is still debated. Alternative monoclinic, triclinic [23] or non-centrosymmetric $\text{Pna}2_1$ orthorhombic [20-22] space groups have been suggested. Noteworthy, the \mathbf{k}, \mathbf{p} modelling of such phases should take into account the loss of inversion symmetry.

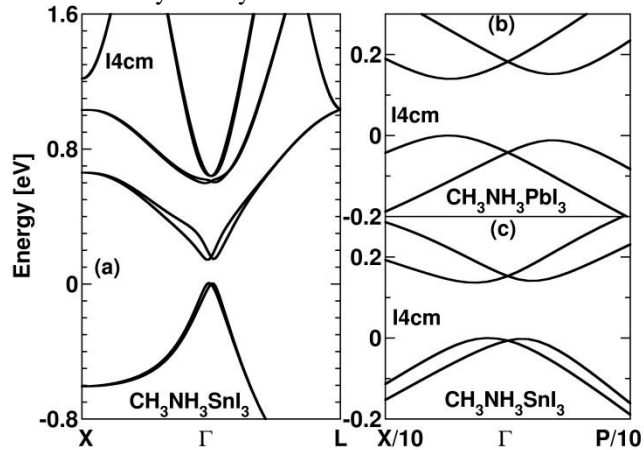


Figure 4 (a) Band structure of the I4cm phase of $\text{CH}_3\text{NH}_3\text{SnI}_3$ with SOC and zoom close to the critical Γ point, (b) for $\text{CH}_3\text{NH}_3\text{PbI}_3$ and (c) for $\text{CH}_3\text{NH}_3\text{SnI}_3$.

4 Summary and outlook In the present work, we have thoroughly investigated different phases of tin and lead based HOP and their all-inorganic analogues, with special attention on the room temperature phases relevant for photovoltaic applications. Based on both DFT and \mathbf{k}, \mathbf{p} approaches, we confirm the importance of SOC for an accurate description of band edge states in this class of materials. The fundamental optical absorption of these materials is associated to transitions between a doubly degenerate spin-orbit split-off CB and a doubly degenerate VB. The spin-orbit splitting of the CB of the tin halide materials is about three times smaller than the one of lead halide compounds. The hole conduction of these materials is related to a quasi-isotropic VB dispersion and a small effective mass. Both the high temperature phase sequence of CsSnI_3 leading to the room temperature orthorhombic γ -phase and the α and β -phases of $\text{CH}_3\text{NH}_3\text{MI}_3$ HOPs, reported recently, are analysed starting from the ideal cubic phase using DFT calculations and a \mathbf{k}, \mathbf{p} perturbative approach. The effect of strain is systematically smaller than that induced by SOC. The loss of inversion symmetry in presence of strong SOC yields further splitting of the electronic bands away from the critical points, especially for the room temperature I4cm phase of $\text{CH}_3\text{NH}_3\text{PbI}_3$. Except for reversed band edge states ordering and strong SOC, these compounds show many similarities with conventional semiconductors, leading to new class of semiconductors different from absorbers commonly used in DSSC.

Acknowledgements This work was performed using HPC resources from GENCI-CINES/IDRIS grant 2013-c2013096724.

The work is supported by Agence Nationale pour la Recherche (PEROCAI project ANR-10-04).

References

- [1] D.B. Mitzi, S. Wang, C.A. Field, C.A., Chess and A.M. Guloy, *Science* **267**, 1473 (1995).
- [2] A. Kojima, K. Teshima, Y. Shirai and T. Miyasaka, *J. Am. Chem. Soc.* **131**, 6050 (2009).
- [3] M. M. Lee, J. Teuscher, T. Miyasaka, T. N. Murakami and H. J. Snaith, *Science* **338**, 643 (2012).
- [4] A. Feltrin and A. Freundlich, *Renewable Energy* **33**, 180 (2008).
- [5] S. Almosni, C. Robert, T. Nguyen Thanh, C. Cornet, A. Létoublon, T. Quinci, C. Levallois, M. Perrin, J. Kuyyalil, L. Pedesseau, A. Balocchi, P. Barate, J. Even, J.-M. Jancu, N. Bertru, X. Marie, O. Durand and A. Le Corre, *J. Appl. Phys.* **113**, 123509 (2013).
- [6] J. H. Heo, S. H. Im, J. H. Noh, T. N. Mandal, C. S. Lim, J. A. Chang, Y. H. Lee, H. J. Kim, A. Sarkar, M. K. Nazeeruddin, M. Grätzel and S. I. Seok, *Nature Photonics* **7**, 487 (2013).
- [7] J. Burschka, N. Pellet, S. J. Moon, R. Humphry-Baker, P. Gao, M. K. Nazeeruddin, M. Grätzel, *Nature* **499**, 316 (2013).
- [8] J. H. Noh, S. H. Im, J. H. Heo, T. N. Mandal and S. I. Seok, *Nano Lett.* **13**, 1764 (2013).
- [9] M. Liu, M. B. Johnston and H. J. Snaith, *Nature* **501**, 395 (2013).
- [10] H.-S. Kim, I. Mora-Sero, V. Gonzalez-Pedro, F. Fabregat-Santiago, E. J. Juarez-Perez, N.-G. Park and J. Bisquert, *Nature Comm.* **4**, 2242 (2013).
- [11] N. G. Park, *J. Phys. Chem. Lett.* **4**, 2423 (2013).
- [12] B. Oregan and M. A. Grätzel, *Nature* **353**, 737 (1991).
- [13] J. Even, L. Pedesseau, J.-M. Jancu, and C. Katan, *J. Phys. Chem. Lett.* **4**, 2999 (2013).
- [14] J. Even, L. Pedesseau, M.-A. Dupertuis, J.-M. Jancu, and C. Katan, *Phys. Rev. B* **86**, 205301 (2012).
- [15] I. Chung, J.-H. Song, J. Im, J. Androulakis, C. D. Malliakas, H. Li, A. J. Freeman, J. T. Kenney and M. G. Kanatzidis, *J. Am. Chem. Soc.* **134**, 8579 (2012).
- [16] I. Chung, B. Lee, J. He, R. P. H. Chang and M. G. Kanatzidis, *Nature*, **485**, 486 (2013).
- [17] I. Borriello, G. Cantele and D. Ninno, *Phys. Rev. B* **77**, 235214 (2008).
- [18] K. Yamada, S. Funabiki, H. Horimoto, T. Matsui, T. Okuda and S. Ishida, *Chem. Lett.* 804 (1991).
- [19] D. M. Trots and S. V. Myagkota, *J. Phys. Chem. Solids* **69**, 2520 (2008).
- [20] A. Poglitsch and D. Weber, *J. Chem. Phys.* **87**, 6373 (1987).
- [21] T. Baikie, Y. Fang, J. M. Kadro, M. Schreyer, F. Wei, S. G. Mhaisalkar, M. Graetzel and T. J. White, *J. Mater. Chem. A* **1**, 5628 (2013).
- [22] Y. Kawamura, H. Mashiyama, K. Hasebe, *J. Phys. Soc. Jpn.* **71**, 1694 (2002).
- [23] C. C. Stoumpos, C. D. Malliakas and M. G. Kanatzidis, *Inorg. Chem.* **52**, 9019 (2013).
- [24] I. P. Swainson, R. P. Hammond, C. Soulliere, O. Knop, W. Massa, *J. Solid State Chem.* **176**, 97 (2003).
- [25] X. Gonze, J.-M. Beuken, R. Caracas, F. Detraux, M. Fuchs, G.-M. Rignanese, L. Sindic, M. Verstraete, G. Zerah, F. Jollet, M. Torrent, A. Roy, M. Mikami, P. Ghosez, J.-Y. Raty, and D. Allan, *Computational Materials Science* **25**, 478 (2002).
- [26] C. Hartwigsen, S. Goedecker and J. Hutter, *Phys. Rev. B* **58**, 3641 (1998).
- [27] elkfp-lapwcode, "<http://elk.sourceforge.net/>
- [28] J. P. Perdew, K. Burke and M. Ernzerhof, *Phys. Rev. Lett.* **77**, 3865 (1996).
- [29] M. van Schilfhaarde, T. Kotani and S. Faleev, *Phys. Rev. Lett.* **96**, 226402 (2006).
- [30] I. Vurgaftman, J. R. Meyer, and L. R. Ram-Mohan, *J. Appl. Phys.* **89**, 5815 (2001).
- [31] N. Chimot, J. Even, H. Folliot and S. Lualiche, *Physica B* **364**, 263 (2005).